Detrital rutile ages can deduce the tectonic setting of sedimentary basins

Inês Pereira, Craig Storey, Robin Strachan, Telmo Bento dos Santos, James Darling

Detrital rutile ages can deduce the tectonic setting of sedimentary basins

Inês Pereira[1*] Craig Storey[1] Robin Strachan[1] Telmo Bento dos Santos[2,3] James Darling[1]

[1] School of the Environment, Geography and Geosciences, University of Portsmouth, Portsmouth, PO1 3QL, Hampshire, United Kingdom

[2] FCUL – Faculdade de Ciências, Universidade de Lisboa, Campo Grande, 1749–016, Lisboa, Portugal

[3] Instituto Dom Luiz (IDL), Faculdade de Ciências, Universidade de Lisboa, Campo Grande, 1749–016, Lisboa, Portugal

*corresponding author: ines.pereira@port.ac.uk

Graphical abstract

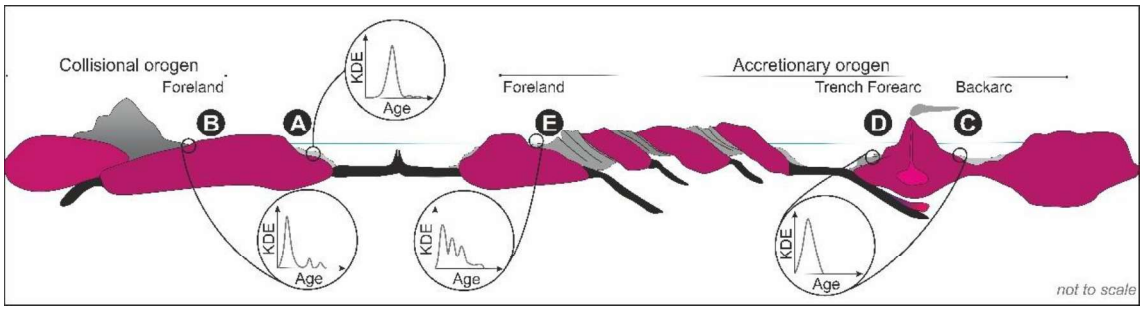

Highlights

- Detrital rutile age distributions are sensitive to tectonic environments
- A new tool to discriminate the tectonic setting of sedimentary basins
- Rutile can distinguish different foreland basins and extensional settings
- We test this tool using well-characterised Precambrian basins
- This tool might be applied to units that endured tectonothermal overprinting events

Abstract

Sedimentary sequences contain a detailed record of the evolution of the Earth's surface. Detrital mineral grains provide, for example, evidence of source redox

conditions, insights into the age, geochemistry and petrology of basement sources and can also be used to elucidate tectonic environments. Detrital zircon has been used as a means of analysing the tectonic setting of host sedimentary successions, but with potentially ambiguous results. It is important to find additional ways to discriminate depositional settings, particularly in Precambrian sequences where other proxies are either not available or have been lost. In this contribution we provide a new way to discriminate between different sedimentary tectonic environments using the mineral rutile. We present a large compilation of detrital rutile data to show that the U-Pb age distribution is sensitive to the tectonic setting of the basin in which the host sediments were deposited. We then apply this new approach to two case studies, where the depositional setting and age are well-constrained: siliciclastic units of NW Scotland which were deposited in the Neoproterozoic foreland of the Grenville Orogen and on the Cambrian passive margin of the Iapetus Ocean, and the Brazilian Sabará basin located within the Palaeoproterozoic foreland of the Minas orogen. We compare the detrital rutile and zircon age distributions of these successions, showing that in some cases they are different, and that rutile is most sensitive to the youngest metamorphic events affecting the sources, reinforcing the applicability of this tool. By testing this new method on polyphasally-deformed successions (Sabará basin) we show that detrital rutile can still inform the tectonic setting even at medium grades of metamorphism.

Keywords: plate tectonics; sedimentary basins; rutile; foreland; tectonic discrimination

1. INTRODUCTION

Although modern sedimentary basins only account for 16% of the terrestrial land surface, river catchments drain 67% of the global non-glaciated land surface to a terrestrial sink (Nyberg et al., 2018), thus making the terrestrial sedimentary record highly representative of the exposed continental crust at the time of deposition. As the

sedimentary record goes back as far as 3.8 Ga (Fedo et al., 2001) and is more temporally complete than the igneous record (Cavosie et al., 2005), it is a repository of valuable geological information. It has provided, for example, evidence related to the evolution of the continental crust (Dhuime et al., 2017) and the nature of now-vanished Hadean crust (Cavosie et al., 2005).

With the increasing ability of many laboratories to analyse and process large amounts of geochronological data, detrital zircon studies have proliferated. Multi-isotopic proxies in zircon, including U, Pb, Th, Hf, O, can provide insight into not only age of crystallisation, but also magma composition, timing of extraction of the source from the depleted mantle reservoir, and constraints on crustal recycling, which have helped to understand early Earth processes (*e.g.* Bradley, 2011; Condie and Kröner, 2013). Detrital zircon studies have contributed towards paleogeographical reconstructions (e.g. Belousova et al., 2002; Mulder et al., 2018), and have been used to elucidate tectonic settings of sedimentary basins (Cawood et al., 2012).

However, information derived from detrital zircons can bias our understanding of the evolution of continents and sedimentary basins, as it preferentially records syn- to late-orogenic felsic magmatism (e.g. Condie, 2014; Spencer et al., 2015). Generation of zircon-bearing felsic magma can also take place during rifting and lithospheric extension, which leads to uncertainties when applying tectonic discrimination diagrams based on zircon. In the absence of fossils and environmental-specific markers, determining depositional tectonic settings in Precambrian sequences is challenging and thus it is important to find new proxies. An alternative way of tackling this problem is by looking at other components of the detrital record that form as a response to tectonic processes, such as metamorphic minerals, which may provide a clearer link to convergent and collisional-related basins.

Convergent- or collisional-related tectonics generally results in regional Barrovian-style metamorphism, in contrast to extensional tectonics where any associated metamorphism (if present at all) is low-pressure in nature (Robinson, 1987).

Therefore, by using a metamorphic mineral that is stable at a wide range of pressures and temperatures, mechanically and chemically robust, can endure sedimentary cycles of transport and diagenesis, and is amenable for high-resolution isotopic dating, it may be possible to discriminate between sedimentary basins formed in convergent/collisional and extensional settings.

Rutile is commonly found in siliciclastic rocks and, together with zircon and tourmaline, can be used to define a sediment maturity index (Hubert, 1962). Rutile can grow in a range of P-T metamorphic conditions (*e.g.* Angiboust and Harlov, 2017; Liou et al., 1998; Hart et al., 2018), but more rarely at greenschist and amphibolite facies (Luvizotto et al., 2009b). Rutile is therefore expected to form commonly during subduction and collision associated with orogenesis and less frequently during extensional tectonics. In continental collision zones, higher pressure and temperature conditions tend to exceed the conditions for Pb retentivity in rutile (Cherniak, 2000), affecting a large portion of the continental crust. These conditions largely promote the resetting of the U-Pb isotopic system and new growth of rutile over a relatively short period of time (a few tens of myr). In contrast, accretionary orogens are generally characterised by multiple arc collision events over a longer time frame (potentially hundreds of myr), and are, therefore, likely to result in a more complex rutile age record, comprising multiple sets of metamorphic ages.

In this contribution, we analyse published and new detrital rutile data to show that it can be used to deduce the tectonic setting of sedimentary basins. This new compilation dataset includes detrital rutile from multiple different geographical areas, from both sedimentary rocks and stream sediments. These cover a range of tectonic settings from rift to passive margin, backarc, forearc, accretionary and collisional foreland basins, developed across a wide span of geological time. We apply this new tool to two well-characterised sedimentary units in NW Scotland, with different depositional ages and tectonic settings, whose provenance is relatively well-characterised. In order to test the suitability of this approach to analysing

(meta)sedimentary units with a polyphase tectonometamorphic history we also apply it to sediments deposited in a foreland basin in Brazil during the Palaeoproterozoic.

2.1. Detrital rutile and zircon U-Pb data: what are they recording?

Rutile and zircon can record different aspects of crustal recycling and growth, zircon mostly providing the timing of high-temperature processes, while rutile records peak metamorphism and/or exhumation/cooling histories. In extensional settings, contemporary A-type magmatism can contribute zircon to sedimentary basins (Fig. 1A). However, rutile mostly results from metamorphic reactions and hence would not be expected to form any substantial component of the detrital population in this setting. In collisional settings, due to the higher Pb closure temperature of zircon relative to rutile (zircon in excess of 900˚C while rutile at 570 ˚C, for grains of 100 μm and 1˚C/Ma cooling rates; Cherniak, 2000), zircon ages may include a substantial inherited component (Fig. 1B), whereas rutile often exhibits a distribution curve that reflects the age of the youngest metamorphic event(s) (Fig. 1B).

The frequency age distribution of detrital rutile thus seems to reflect the tectonic depositional environment during the infill of a sedimentary basin. Data from this first large compilation of rutile analyses (Appendix A) are summarised and presented in Figure 2, as a schematic model of the predicted Kernel density estimate (KDE) curves for different tectonic settings.

In convergent-related basins, the rutile KDE's theoretically present a Gaussian distribution curve with the main age peak quite close to the depositional age (Fig.2-C, -D). A more significant rutile population can be expected in association with the accretionary prism in the forearc in comparison with the back of the arc. However, if any rutile is forming due to Barrovian metamorphism imposed on the upper plate, rutile ages from both settings will display a similar Gaussian distribution curve. A similar distribution can be expected from extensional settings, particularly when the detrital

137 rutile population came from a metamorphic source that endured a complete U-Pb rutile
138 resetting. This imparts a unimodal distribution curve, but with the main age peak older
139 than depositional age (Fig. 2-A). Nonetheless, this distribution curve is mostly
140 dependent on the tectonometamorphic events that have affected the source area
141 basement, and could be more complex, with multiple rutile populations instead of just
142 one main age peak.

143 In foreland basins, two types of KDE's can be expected, resembling either a
144 convergent-related KDE (Fig. 2-B) or a multimodal KDE distribution, which reflects only
145 partial resetting in a protracted accretionary history (Fig. 2-E).

146

147 2.2. Detrital rutile cumulative proportion ages and depositional tectonic environments

148

149 To investigate further the suitability of rutile as a proxy in elucidating tectonic
150 environments, we apply the cumulative proportion approach to detrital rutile U-Pb age
151 data. We compare data from different basins, plotting the cumulative proportions of
152 detrital minerals against the growth age minus the estimated depositional age (Fig. 3).
153 This is the same procedure as used by Cawood et al. (2012) for detrital zircon, showing
154 steep curves for collisional-related basins and smooth curves, with large gaps between
155 deposition and growth age for extensional-related basins.

156 A large compilation of detrital rutile U-Pb data is presented as supplementary
157 data (Appendix A), combining sedimentary basins and stream sediment examples
158 associated with different tectonic settings and depositional ages. Cumulative
159 distributions of both rutile and zircon from a backarc and a foreland basin examples are
160 projected in Figure 3 to compare the record from these different minerals. Rutile
161 invariably shows a different distribution to that of zircon, with rutile overlapping quite
162 well with the predicted tectonic field diagram from Cawood et al. (2012), while zircon
163 plots in fields which do not correspond to the true depositional setting of either basin.
164 Thus, it seems that the cumulative distributions of rutile are better proxies than detrital

zircon for discriminating tectonic environments, due to the significant overlap between the different tectonic fields (Cawood et al., 2012), which is a consequence of zircon not being so sensitive to metamorphic processes, and to zircon growth during extensional-related magmatism (Fig. 1A).

Therefore, due to its metamorphic nature and lower Pb-closure temperatures, rutile appears to provide a better means of distinguishing between tectonic environments. In combination with detrital zircon, rutile will lead to better discrimination of depositional tectonic environments in units preserved at low to medium metamorphic grade (sub-upper amphibolite facies). In the next sections, we examine rutile U-Pb datasets from extensional-related, convergent-related and foreland basins.

2.2.1. Extensional basins: rift-passive margins

In extensional settings, rift basins can evolve to passive margin oceanic basins (Fig. 2-A) or infill to produce an aulacogen. Metamorphic rutile is not commonly formed in these settings, and thus this should be reflected in the difference between growth and deposition age. This is the case of a stable continent undergoing extension, such as in North Africa (Nile drainage system during the Cenozoic; Fielding et al., 2018) or in eastern North America (North Carolina; O'Sullivan et al., 2016) where most rutile ages that are significantly older than the depositional age (Fig. 4-A).

Thus, passive margin sediments can typically show an "S" distribution curve, if the extension stage evolved after a continental collision setting. This "S" shape reflects a) no or very little grains formed at the time of deposition, b) a lag that is followed by c) a range of ages contained within a relatively short period, following a Gaussian distribution age. However, due to inherent geological complexity, there are cases more difficult to unravel. For instance, after the amalgamation of Gondwana, during the Neoproterozoic Pan-African Orogeny, certain areas of Gondwana were extended to

192 accommodate the Cambro-Ordovician seas that covered large areas of this
193 supercontinent. Where rifting developed on top of the suture, we refer to these as
194 *'suture rift'* basins. The short time difference between the orogenic event and the
195 development of these basins is reflected in the small gap/lag between the maximum
196 depositional age of these sediments and the age of the youngest rutile (Fig. 4-A, curve
197 2; Rösel et al., 2014a). This, in turn, is reflected in the rutile cumulative proportion
198 curves (Fig. 4B; Avigad et al., 2017). Cambrian rift basins in this context resemble a
199 collisional detrital rutile KDE curve (Fig. 1B) and the cumulative proportion curve
200 overlaps in age difference with the convergent-type curves (Fig. 5). However, as the
201 basin evolves to a passive margin, because there is no generation of metamorphic
202 rutile (due to the unfavourable tectonic setting) the difference between depositional and
203 detrital mineral ages increases. This can be tracked in Cambro-Ordovician sedimentary
204 sequences, with an acute overturn of the cumulative proportion, from base to top,
205 shifting from more than 80% of detrital rutile within a gap of 100 myr in the Cambrian
206 units to about 15% in an equivalent period for the Ordovician units, along with a change
207 in the curve shape (Fig. 4B). Note that the S-shaped curve is an approximation, and
208 that depending on drainage patterns, we should also consider the existence of an
209 important older component decomposing the curve into a double-S shape (Fig. 4; curve
210 1).

211 We acknowledge that in certain circumstances some rutile grains may yield
212 ages similar to the depositional age. This could result from the formation of rutile during
213 hydrothermal activity and/or contact metamorphism or from the resetting of the U-Pb
214 isotopic system during margin hyperextension and basement exhumation.
215 Nonetheless, in most documented examples these relatively young rutile grains only
216 form a minor component of the detrital rutile population (*e.g.* Odlum et al., 2019).

217

218 *2.2.2. Supra-subduction basins*

Clastic sediments deposited in supra-subduction convergent basins are not commonly preserved under low metamorphic conditions, as they are often involved in collisional processes during the ensuing assembly of continents. Typical basins that form at these stages are forearc and backarc basins. Due to the very restricted source availability, usually confined to the exposed arc and potentially the accretionary prism during thickening and thrusting, these basins tend to reflect a unimodal distribution age and the youngest detrital mineral is very close in age to the depositional age (Fig. 2-C,-D). This is the case, despite the small number of rutile grains, of a forearc basin related to the Variscan orogeny (Turkey; Okay et al., 2011) and a backarc basin of Palaeoproterozoic age (Western Australia; Rösel et al., 2014b), showing a very steep rutile cumulative proportion curve with nearly the entire population contained within 100-150 Ma of deposition age. The cumulative age distribution curve resembles more of a “r” in these settings (Fig. 5, curves 1,2).

2.2.3. Foreland basins

Foreland basins develop during collisional orogenesis, associated with accretionary orogens such as arc-continent collision, Cordillera-type or Himalayan-type, collisional orogens (Fig. 2-B,-E). The detrital population distribution in each of these cases reflects its context. The foreland basins of continental collision orogens mainly gather detrital minerals formed as a consequence of very large-scale collision, capturing similar ages with Gaussian age distributions (i.e. recording one main tectonometamorphic event). This is the case for the Pan-African Orogeny (*e.g.* Avigad et al. 2017), recorded in several different basins that accumulated Cambrian sedimentary units deposited during subsequent rifting. A nearly Gaussian age distribution with some inheritance is also a plausible age distribution, such as the detrital rutile distribution associated with the

Himalayan foreland (Fig. 1B). The rutile cumulative proportion distribution ages collected from stream and river sediments in this foreland (Bracciali et al., 2015; 2016) show that about 80% of all grains are within 50 Ma of depositional age, with a smaller inherited component. This can be evaluated in the cumulative proportion distribution as an almost linear curve with a progressive increase in the age difference (Fig. 5, curve 3). The difference between this curve and the Pan-African-type described above is most likely a reflection of the collisional stage at the time of deposition. We can predict that as more of the lower crust is exhumed due to the collisional process, more Himalayan-age metamorphic rutile will reach the foreland basin. This should balance the cumulative proportion curve to nearly 100% within the orogenic period, favouring a Gaussian age distribution.

In the case of accretionary orogens, such as the Cordillera along the eastern margin of the Pacific Ocean, a protracted series of arc-continent collisions will typically result in episodic and prolonged tectono-thermal events and in a multimodal detrital rutile age population (Fig. 2-E). This is shown by the cumulative proportion distribution curves of detrital rutile from the Cretaceous Sevier foreland basin sequences in Utah and Wyoming (Lippert 2014; Fig. 5-curves 4, 5). In this example, there is a nearly continuous generation of metamorphic rutile, with growth age similar to depositional age. Yet, instead of a linear and steep cumulative proportion distribution increase, there is rather a continued stepped growth curve, reflecting a prolonged, but episodic tectonometamorphic history of the source terranes. The gap between depositional age and the youngest rutile ages in the Sevier foreland reflects two different tectonic processes; for the Utah sequence, out of sequence thrusting exposes older basement (white dashed line, Fig. 5), preventing new rutile from reaching the basin, while in the Wyoming sequence, deposition during segmentation of the basin allowed new rutile to reach the foreland.

3. MATERIAL AND METHODS

3.1. Samples

In order to further test the applicability of rutile to the discrimination of tectonic settings of sedimentary basins, we collected new zircon and rutile U-Pb data from three different stratigraphic units, two of which represent foreland basins and the third a passive (extensional) margin basin. Two crop out in NW Scotland, the late Mesoproterozoic to early Neoproterozoic Torridon Group and the Cambrian Ardvreck Group. The third unit crops out in the Quadriláterro Ferrífero in Brazil, the Sabará Formation in the Minas Supergroup. Sample locations, stratigraphic sections and lithological descriptions are presented in Appendix B.

The depositional age of the Torridon Group is constrained to between 997 ± 39 Ma and 1049 ± 46 Ma, and it is interpreted as the siliciclastic infill of the foreland basin of the Grenville orogen (Rainbird et al. 2001; Krabbendam et al. 2017). One sample was collected from the basal Diabaig Formation, and three from the Applecross Formation. The depositional age of the Ardvreck Group is early Cambrian, older than 520 Ma (see Cawood et al. 2007 for details) and it is believed to have accumulated on the extended Laurentian passive margin of the Iapetus Ocean (McKie, 1990). Three samples were collected from Ardvreck Grp., two from the Basal Quartzite Member and one from the Pipe Rock Member. The Sabará Formation (Minas sequence) in Brazil has been interpreted to represent the foreland basin of the Palaeoproterozoic Minas Orogen, deposited during the Rhyacian (Alkmim and Marshak, 1998). Two samples were obtained from the basal metaconglomerate unit.

3.2 Methods

Zircon and rutile U-Pb isotopic data were acquired using an ASI RESOlution 193nm ArF excimer laser coupled to an Analytik Jena Plasma Quant Elite ICP quadrupole MS

at the University of Portsmouth. A summary of the instrumental setup, ablation parameters and conditions can be found in supplementary data (Appendix B).

U-Pb rutile analyses were performed during different analytical sessions with variable parameters, such as spot sizes ranging from 35 to 40 μm, with a laser energy density between 4 and 4.2 J/cm^2 at a repetition rate of 5 Hz. A sample-standard bracketing method was used to correct mass fractionation using R10 rutile as a primary standard (average ID TIMS age of 1091.3 ± 4.7 Ma; Luvizotto et al., 2009a), and three different secondary standards were analysed; R13 (SIMS age of 504 ± 4 Ma; Schmitt and Zack, 2012), R19 (ID TIMS age of 493 ± 10 Ma; Zack et al., 2011) and SAE (unpublished, ID TIMS 495 Ma, provided courtesy of C. Lana, UFOP). Calculated $^{206}Pb/^{238}U$ weighted mean average ages for R13 and R19 secondary standards are within 1.2% accuracy of the reported ages (Appendix C). U-Pb dating of rutile is more difficult than zircon due to overall low U concentration (< 100 ppm) and incorporation of small amounts of Pb at the timing of growth. Common-Pb corrections are not always applicable and natural discordance complicates this further. Filtering these datasets to include only grains that are more than 95% and lower than 105% concordant excludes many grains from these datasets and reduces some of these samples to smaller populations. This might generate a bias in terms of determining precise ages of events, but it is unlikely to have a great effect on the cumulative distributions and the overall distribution curves. No common-Pb corrections were applied.

Zircon U-Pb analyses were performed based on cathodoluminescence images, obtained in a ZEISS EVO10MA Scanning Electron Microscope, in two different sequences using 20 μm ablation spots, with a laser energy density of 3 J/cm^2 at a repetition rate of 2 Hz. A sample-standard bracketing method was used to correct for mass fractionation using BB9 zircon as a primary standard (average ID TIMS age of 560 ± 5 Ma; Santos et al., 2017), and two different secondary standards were analysed; 91500 zircon (ID-TIMS of 1065 ± 5 Ma; Wiedenbeck et al., 1995) and KAAP

Valley tonalite zircon (SHRIMP age yielding 3226 ± 14 Ma; Armstrong et al., 1990). A concordia age yielding 1050.4 ± 4.9 Ma for 91500 and an upper intercept age of 3222 ± 28 Ma for Kaap Valley tonalite zircon are within uncertainties of reported ages (Appendix D).

All data were processed using the software package IOLITE 3.31. Concordia, weighted mean average ages, age frequency histograms and cumulative probability distributions were calculated using ISOPLOT/EX 4.1 (Ludwig, 2009), *detzrcr* R-package (Andersen et al., 2018) and Microsoft Excel. Statistical tests applied to the detrital populations were conducted using DZstats, a Matlab-based application (Saylor and Sundell, 2016). New U-Pb data is presented as supplementary data (Appendix C and D).

4. RESULTS AND DISCUSSION

Detrital rutile and zircon U-Pb ages are presented and discussed using only the ± 5% discordant data, which increases the confidence in the ages used and their significance. This is particularly relevant for Palaeoproterozoic, Archaean and Hadean mineral ages, where variable degrees of Pb-loss or age mixing can produce concordant isotopic ratios but meaningless geological ages (Pereira et al., 2019). $^{206}Pb/^{238}U$ ages are used for ages of < 1000 Ma and $^{207}Pb/^{206}Pb$ ages are used for ages of > 1000 Ma. We apply cross-correlation metrics to assess similarity or dissimilarity between different populations (Saylor and Sundell, 2016).

4.1. The NW Scotland case study

The new detrital rutile U-Pb age data presented here for the Torridon and Ardvreck groups are integrated with published U-Pb analyses. The U-Pb zircon ages of the Applecross Formation are those reported from Lancaster et al. (2011) and zircon and

rutile U-Pb data from Krabbendam et al. (2017), while for the Diabaig Formation our new detrital U-Pb ages for both zircon and rutile (Appendix C, D) are combined with the zircon data of Kinnaird et al. (2007). For the Ardvreck Group, zircon data has been compiled from Cawood et al. (2007) and Lancaster et al. (2011). CL zircon images are shown in appendix E.

4.1.1. Late Mesoproterozoic to early Neoproterozoic Torridon Group

From the Torridon Group, we analysed samples of the Diabaig Formation and the Applecross Formation. From the Diabaig Formation (Fig. 6A and C) we analysed 55 rutile grains, retrieving 35 concordant grains, and 135 zircon grains (103 grains were concordant). The youngest rutile in the Diabaig Formation is 1089 ± 29 Ma (4% discordant) whilst the oldest rutile is 1896 ± 25 Ma (1% discordant). From the Applecross Formation (Fig. 6B and D) we analysed 266 rutile grains (145 concordant grains) and combined them with 275 zircon grains (191 concordant grains). The youngest rutile in the Applecross Formation is 1018 ± 50 Ma (0% discordant) whilst the oldest rutile is 2733 ± 37 Ma (3% discordant).

By applying different statistical tests, including cross-correlation, Likeness and Similarity tests (as in Saylor and Sundell, 2016), we demonstrate that the frequency distribution of both rutile populations from the Torridon Group are significantly similar (Table 1).

As for the detrital zircon datasets, both units have different population distributions: the Diabaig Formation exhibits a significant Neoarchaean age peak, while the Applecross Formation shows a multimodal distribution, with a major age peak between 1.8 and 1.65 Ga. The oldest zircon grain is found in the Diabaig Formation yielding an age of 3495 ± 19 Ma (3% discordant). This is supported by the statistical tests, showing low cross-correlation coefficients (Table 1) between these detrital zircon populations.

Currently, the general view is that the Diabaig Formation was deposited in localised basins that developed immediately above the regional unconformity with the underlying Lewisian Gneiss Complex (Kinnaird et al., 2007; Stewart, 2002). In this context, it might be expected that the sediments would preserve a close record of the dominant Archaean-Palaeoproterozoic tectonothermal events that characterise this basement. However, the presence of many Mesoproterozoic-aged rutile grains in both the Diabaig and the Applecross formations indicates a more distal source from the Lewisian Gneiss Complex which lacks such Mesoproterozoic ages. This is consistent with the general westerly source invoked for the Torridon Group as a whole (Stewart, 2002; Kinnaird et al., 2007: Krabbendam et al., 2017). The evolution of the Diabaig-Applecross basin appears to have favoured the inclusion of increasingly younger detritus up-section, presumably more distal. Thus, the proportion of late Archaean material decreases upwards at the expense of increasing proportions of Palaeo- and Mesoproterozoic zircon and rutile grains.

The cumulative probability curves of rutile and zircon in the Diabaig Formation (Fig. 6C) are quite different from those for the Applecross Formation (Fig. 6D) and supported by the low cross-correlation coefficients (Table 1). While in the Applecross Formation dataset, the differences between rutile and zircon can be explained by their contrasting closure temperatures, with zircon recording crystallisation/metamorphic ages while rutile records exhumation and cooling, this is not plausible for the Diabaig Formation curves. Two different hypotheses could explain these differences: 1) a variation in the proportions of detritus eroded from two distinct basement sources (*e.g.* Archaean Lewisian Gneiss Complex and a metamorphic Mesoproterozoic source), or 2) a complete resetting of U-Pb systematics in existing rutile and/or growth of new rutile in a single reworked basement source of Archaean age. The former would imply distinct palaeocurrents, which would carry sediments from multiple sources. This is inconsistent with the main easterly-flowing palaeocurrents recorded within the Diabiag and Applecross successions (Stewart, 2002), despite some local variability in Diabaig

palaeocurrents. The second hypothesis implies a variation in the basement source area from the Diabaig to Applecross formations. A feasible interpretation is that the Diabaig Formation contains detritus derived from external sectors of the Grenville belt characterised by Archaean protoliths that had been reworked at 1.6-1.0 Ga (such as the Gagnon Terrane; van Gool et al., 2008). This source would contribute mostly Archaean zircon and Proterozoic metamorphic rutile. As fluvial systems progressively cut back into the orogenic hinterland they would have eroded younger accreted Ketilidian/Labradorian terranes that had also potentially been reworked at this time. This source would then also contribute Proterozoic zircon and thus explain the shift of zircon age peaks as seen from the Diabaig to the Applecross formations. These variations can be envisaged in terms of protolith fertility (for zircon and/or rutile) and mixing of detrital components from variable sources in the eastern Grenvile Province.

4.1.2. Cambrian Eriboll Formation

Three samples from the basal siliciclastic unit of the Ardvreck Group were collected, including the Basal Quartzite Member (BQ; Fig 7A and C) and the bioturbated Pipe Rock Member. (PR; Fig 7B and D). From the BQ, we collected data from 263 rutile grains retrieving 112 concordant grains and combined them with 123 zircon grains (81 concordant grains). The youngest rutile in BQ is 1006 ± 78 Ma (5% discordant), yet the youngest cluster occurs at ca. 1.6 Ga. The oldest rutile is 2953 ± 36 Ma (3% discordant). In the PR we collected data from 222 rutile grains (120 concordant grains) and combined them with 158 zircon grains (99 of which were concordant). The youngest rutile in PR is 1526 ± 98 Ma (2% discordant) whilst the oldest rutile is 2755 ± 96 Ma (2% discordant).

The frequency distribution of both detrital rutile populations is compared using different statistical tests (Table 1). The very minor late Mesoproterozoic rutile grain

441 contribution disappears from BQ into PR, with a proportional increase of Archaean age
442 rutile. The detrital zircon populations, however, show a different distribution to that of
443 rutile, yielding low cross-correlations (Table 1).

444 In BQ, detrital zircon yields only Archaean ages. In PR, the Eo- and
445 Palaeoarchaean populations decrease in favour of an increasing late
446 Palaeoproterozoic source. The cumulative probability curves of BQ (Fig. 7C) are
447 distinct from the PR equivalent (Fig. 7D). Rutile and zircon distribution curves are
448 statistically different (table 1) but, considering their differences, both units show a
449 similar variation. In BQ, the difference between the lower and upper quartiles for both is
450 of about the same range of time, ca. 200 Ma, with absolute ages shifted between rutile
451 and zircon. These can be interpreted as near complete resetting of the rutile population
452 in the source of BQ. PR is different, with both detrital minerals exhibiting two important
453 modes and a generalised increase of younger Mesoproterozoic rutiles. There are two
454 options for interpreting these observations: either near complete resetting and/or
455 cooling of the late Palaeoproterozoic source of PR, or partial resetting of both the late
456 Archaean and Palaeoproterozoic sources during the Palaeo-Mesoproterozoic.

457 Detrital zircons from BQ and PR have Eo- and Palaeoarchaean Hf model ages,
458 with an important line of extraction at ca 3.3 Ga, but model crustal residence ages
459 (TDM) as old as 3.6 and 4.0 Ga (Lancaster et al., 2015). This indicates an older and
460 more distal source than the mainly Neoarchaean Lewisian Gneiss Complex (Fig. 1b in
461 Appendix B). A SE-directed paleoflow (McKie, 1990) supports a source to the NW,
462 most probably east Greenland (Cawood et al., 2007). However, the 1.7 – 1.65 Ga rutile
463 age peak can only be reconciled with this source if during the Nagssugtoqidian
464 orogeny, rutile formed/reset in a slowly cooled terrane (to account for the ca. 150 Ma
465 difference between zircon and rutile ages). These ages are within the range of recently
466 reported metamorphic rutile ages from the Nagssugtoqidian in SE Greenland (Müller et
467 al., 2018) which reinforces our interpretation. It is worthwhile noting that although the

468 BQ samples were collected within a few metres of the underlying Applecross Formation
469 there is no major reworking of the Torridon Group. This suggests a long period of
470 erosion and induration of the Torridon Group prior to the Cambrian marine
471 transgression which likely occurred relatively rapidly across a peneplained surface.
472 The detrital rutile and zircon cumulative probability curves exhibit a well-
473 developed “S” shape for the Basal Quartzite Member but a more complex double-“S”
474 form for the Pipe Rock Member. The latter might be due to sourcing of basement
475 sources that underwent a more protracted orogenic evolution, such as the terranes in
476 Greenland. Nonetheless, both distribution curves are consistent with the extensional
477 (passive margin) setting indicated by the geological evidence.
478 We have therefore shown that the new tool we propose (section 2.2)
479 discriminates between these two stratigraphic units from NW Scotland, thus reinforcing
480 its applicability to Archaean or Palaeoproterozoic stratigraphic sequences, and
481 illustrating how it can unravel the protracted evolution of the sources that contributed to
482 these basins.
483
484 4.2. Brazil case study
485
486 To verify if this tool can be applied to geologically more complex metasedimentary
487 units, we have analysed the detrital rutile population from the Sabará Formation that
488 was deposited during the Rhyacian in the foreland basin of the Minas orogen (Alkmim
489 and Marshak, 1998). The maximum depositional age of this unit has been constrained
490 at ca. 2121 Ma, a minimum depositional age of 2060 Ma and the detrital zircon U-Pb
491 distribution exhibits two important clusters, one at 2950-2650 Ma and another at 2320-
492 2160 Ma (Martínez Dopico et al., 2017). We retrieved 59 grains from 2 samples, from
493 which only 12 yield concordant ages (within 5% discordance; Appendix C). Because
494 this unit was affected by a late Neoproterozoic to Cambrian tectonometamorphic event,

495 many rutile grains record variable Pb-loss with a lower intercept age of 490 ± 30 Ma
496 (MSWD = 0.66; Fig. 8A) compatible with the collapse stages of the Brasiliano event.
497 By combining Tera-Wasserburg $^{207}Pb/^{206}Pb$ regression ages, $^{207}Pb/^{206}Pb$
498 intercept ages with naturally concordant rutile data we compare the KDE distribution of
499 detrital rutile (this study) with that of zircon (Martínez Dopico et al. 2017; Fig. 8B). Due
500 to the limited number of grains, retrieved ages only partly represent the entire
501 population. Yet, the distribution of rutile ages resembles that of zircon (Fig. 8B), with a
502 0.855 cross-correlation using their respective KDEs. Concordant ages are between
503 2929 Ma and 2125 Ma.
504 The detrital rutile and zircon cumulative distributions are quite similar (Fig. 8C),
505 resembling a cumulative distribution curve such as the Himalayan foreland (Fig. 5,
506 curve 5). Agreement between the detrital cumulative age distribution and evidence for
507 the synorogenic tectonic setting (Alkmim and Marshak, 1998) demonstrates the
508 suitability of this tool applied to geologically complex settings, despite rutile being prone
509 to partial or full resetting under higher than low amphibolite metamorphic grade
510 conditions.
511
512 4.3. Summary
513
514 We have compared detrital zircon and rutile distribution ages from three sedimentary
515 basins of known tectonic setting. In each case, the rutile distribution ages are
516 consistent with the known tectonic setting and furthermore have provided insights into
517 the nature and tectonothermal evolution of source regions. Rutile U-Pb distribution
518 ages are often offset towards the youngest recorded events, and where protolith and
519 metamorphic conditions enable rutile growth, this mineral will better record the
520 youngest metamorphic/magmatic event affecting the basement source prior to
521 weathering and final deposition in the sedimentary basin. Therefore, detrital rutile
522 cumulative distribution ages, as shown in these case-studies, are reliable in

discriminating distinct tectono-sedimentary settings. A summary of rutile cumulative probability curves, including new data presented here, is shown in Figure 9.

5. CONCLUSIONS

The importance of rutile lies in its sensitivity to tectonometamorphic processes. In this contribution, we have shown how the age distribution of detrital rutile can help to elucidate the tectonic environment at the time of deposition, complementing interpretations based on detrital zircon. This powerful new tool can be applied to the geological record with the aim of identifying the tectonic settings of depositional basins, and it can also provide insight into tectonic processes affecting source terrains, as shown by our case study of the Cambrian succession in NW Scotland. In detail, it can be used to discriminate between extensional and collisional basins, and moreover different types of collision-related basins. For example, detrital rutile grains from a succession deposited in the foreland of an accretionary orogen will typically record a prolonged metamorphic history (*e.g.* the Sevier), while a succession deposited adjacent to a major continental collision zone will mainly record the final collision stage (*e.g.* the Himalaya). However, intrinsic geologic complexities such as discussed for the Sevier foreland and rifting location (*e.g.* Cambrian successions in North African localities) can potentially complicate understanding of the tectonic environment at the time of deposition. In such cases, we have shown how useful it may be to compare the detrital rutile cumulative proportion distribution curves of a complete sequence and characterise changes in the cumulative distribution curve shape.

By applying this new tool to Precambrian stratigraphic sequences, we provide a new means of recognising convergent and collisional basins in the geological record. This new tool is likely to be of particular value when applied to parts of the geological record characterised by only fragmentary exposure such as the Archaean and Palaeoproterozoic cratons. The detrital rutile record could therefore provide critical

551 evidence towards the understanding of early Earth tectonics and basin settings, which
552 are key in reconstructions targeting the geodynamic evolution of our planet.
553
554 Acknowledgments
555
556 IP wants to thank the University of Portsmouth for providing a PhD bursary, technical
557 support and for funding all analytical work. Fernando F. Alkmim and Mike Dunk are
558 thanked for support during fieldwork. TBS was supported by FCT—Project
559 UID/GEO/50019/2019—Instituto Dom Luiz. We are thankful for Margo Odlum's
560 thorough revision and for efficient editorial handling by An Yin.
561
562 References
563 Alkmim, F.F., Marshak, S., 1998. Transamazonian Orogeny in the Southern São
564 Francisco Craton Region, Minas Gerais, Brazil: evidence for Paleoproterozoic
565 collision and collapse in the Quadrilátero Ferrífero. Precambrian Res. 90, 29–58.
566 https://doi.org/10.1016/S0301-9268(98)00032-1
567 Andersen, T., Kristoffersen, M., Elburg, M.A., 2018. Visualizing, interpreting and
568 comparing detrital zircon age and Hf isotope data in basin analysis - a graphical
569 approach. Basin Res. 30, 132–147. https://doi.org/10.1111/ijlh.12426
570 Armstrong, R.A., Compston, W., de Wit, M.J., Williams, I.S., 1990. The stratigraphy of
571 the 3.5-3.2 Ga Barberton Greenstone Belt revisited: a single zircon ion microprobe
572 study. Earth Planet. Sci. Lett. 101, 90–106.
573 Avigad, D., Morag, N., Abbo, A., Gerdes, A., 2017. Detrital rutile U-Pb perspective on
574 the origin of the great Cambro-Ordovician sandstone of North Gondwana and its
575 linkage to orogeny. Gondwana Res. 51, 17–29.
576 https://doi.org/10.1016/j.gr.2017.07.001
577 Belousova, E. a., Griffin, W.L., O'Reilly, S.Y., Fisher, N.I., 2002. Igneous zircon: trace
578 element composition as an indicator of source rock type. Contrib. to Mineral.

579 Petrol. 143, 602–622. https://doi.org/10.1007/s00410-002-0364-7
580 Bracciali, L., Najman, Y., Parrish, R.R., Akhter, S.H., Millar, I., 2015. The Brahmaputra
581 tale of tectonics and erosion: Early Miocene river capture in the Eastern Himalaya.
582 Earth Planet. Sci. Lett. 415, 25–37. https://doi.org/10.1016/j.epsl.2015.01.022
583 Bracciali, L., Parrish, R.R., Najman, Y., Smye, A., Carter, A., Wijbrans, J.R., 2016. Plio-
584 Pleistocene exhumation of the eastern Himalayan syntaxis and its domal 'pop-up.'
585 Earth-Science Rev. 160, 350–385. https://doi.org/10.1016/j.earscirev.2016.07.010
586 Bradley, D.C., 2011. Secular trends in the geologic record and the supercontinent
587 cycle. Earth-Science Rev. 108, 16–33.
588 https://doi.org/10.1016/j.earscirev.2011.05.003
589 Cavosie, A.J., Valley, J.W., Wilde, S.A., 2005. Magmatic δ18O in 4400-3900 Ma
590 detrital zircons: A record of the alteration and recycling of crust in the Early
591 Archean. Earth Planet. Sci. Lett. 235, 663–681.
592 https://doi.org/10.1016/j.epsl.2005.04.028
593 Cawood, P.A., Nemchin, A.A., Strachan, R., 2007. Provenance record of Laurentian
594 passive-margin strata in the northern Caledonides: Implications for paleodrainage
595 and paleogeography. Bull. Geol. Soc. Am. 119, 993–1003.
596 https://doi.org/10.1130/B26152.1
597 Cawood, P.A., Hawkesworth, C.J., Dhuime, B., 2012. Detrital zircon record and
598 tectonic setting. Geology 40, 875–878. https://doi.org/10.1130/G32945.1
599 Cherniak, D.J., 2000. Pb diffusion in rutile. Contrib. Miner. Pet. 139, 198–207.
600 https://doi.org/10.1016/S0009-2541(00)00233-3
601 Condie, K.C., 2014. Growth of continental crust: a balance between preservation and
602 recycling. Mineral. Mag. 78, 623–637.
603 https://doi.org/10.1180/minmag.2014.078.3.11
604 Condie, K.C., Kröner, A., 2013. The building blocks of continental crust: Evidence for a
605 major change in the tectonic setting of continental growth at the end of the
606 Archean. Gondwana Res. 23, 394–402. https://doi.org/10.1016/j.gr.2011.09.011

607 Dhuime, B., Hawkesworth, C.J., Delavault, H., Cawood, P.A., 2017. Continental growth
608 seen through the sedimentary record. Sediment. Geol. 357, 16–32.
609 https://doi.org/10.1016/j.sedgeo.2017.06.001
610 Fedo, C.M., Myers, J.S., Appel, P.W.U., 2001. Depositional setting and
611 paleogeographic implications of earth's oldest supracrustal rocks, the >3.7 Ga
612 Isua greenstone belt, West Greenland. Sediment. Geol. 141–142, 61–77.
613 https://doi.org/10.1016/S0037-0738(01)00068-9
614 Fielding, L., Najman, Y., Millar, I., Butterworth, P., Garzanti, E., Vezzoli, G., Barfod, D.,
615 Kneller, B., 2018. The initiation and evolution of the River Nile. Earth Planet. Sci.
616 Lett. 489, 166–178. https://doi.org/10.1016/j.epsl.2018.02.031
617 Hart, E., Storey, C., Bruand, E., Schertl, H.P., Alexander, B.D., 2016. Mineral
618 inclusions in rutile: A novel recorder of HP-UHP metamorphism. Earth Planet. Sci.
619 Lett. 446, 137–148. https://doi.org/10.1016/j.epsl.2016.04.035
620 Hart, E., Storey, C., Harley, S.L., Fowler, M., 2018. A window into the lower crust:
621 Trace element systematics and the occurrence of inclusions/intergrowths in
622 granulite-facies rutile. Gondwana Res. 59, 76–86.
623 https://doi.org/10.1016/j.gr.2018.02.021
624 Hubert, J.F., 1962. A Zircon-Tourmaline-Rutile Maturity Index and the Interdependence
625 of the Composition of Heavy Mineral Assemblages with the Gross Composition
626 and Texture of Sandstones. J. Sediment. Petrol. 32, 440–450.
627 Kinnaird, T.C., Prave, A.R., Kirkland, C.L., Horstwood, M., Parrish, R., Batchelor, R.A.,
628 2007. The late Mesoproterozoic-early Neoproterozoic tectonostratigraphic
629 evolution of NW Scotland: the Torridonian revisited. J. Geol. Soc. London. 164,
630 541–551. https://doi.org/10.1144/0016-76492005-096
631 Krabbendam, M., Bonsor, H., Horstwood, M.S.A., Rivers, T., 2017. Tracking the
632 evolution of the Grenvillian foreland basin: Constraints from sedimentology and
633 detrital zircon and rutile in the Sleat and Torridon groups, Scotland. Precambrian
634 Res. 295, 67–89. https://doi.org/10.1016/j.precamres.2017.04.027

635 Lancaster, P.J., Storey, C.D., Hawkesworth, C.J., Dhuime, B., 2011. Understanding the
636 roles of crustal growth and preservation in the detrital zircon record. Earth Planet.
637 Sci. Lett. 305, 405–412. https://doi.org/10.1016/j.epsl.2011.03.022
638 Lippert, P.G., 2014. Detrital U-Pb geochronology provenance analyses: case studies in
639 the Greater Green River Basin, Wyoming, and the Book Cliffs, Utah. University of
640 Kansas, 253p.
641 Ludwig, K.R., 2009. User's Manual for Isoplot 4.15. A Geochronological Toolkit for
642 Microsoft Excel. Berkeley Geochronol. Cent. Spec. Publ. 76.
643 Luvizotto, G.L., Zack, T., Meyer, H.P., Ludwig, T., Triebold, S., Kronz, A., Münker, C.,
644 Stockli, D.F., Prowatke, S., Klemme, S., Jacob, D.E., von Eynatten, H., 2009a.
645 Rutile crystals as potential trace element and isotope mineral standards for
646 microanalysis. Chem. Geol. 261, 346–369.
647 https://doi.org/10.1016/j.chemgeo.2008.04.012
648 Luvizotto, G.L., Zack, T., Triebold, S., Von Eynatten, H., 2009b. Rutile occurrence and
649 trace element behavior in medium-grade metasedimentary rocks: Example from
650 the Erzgebirge, Germany. Mineral. Petrol. 97, 233–249.
651 https://doi.org/10.1007/s00710-009-0092-z
652 Martínez Dopico, C.I., Lana, C., Moreira, H.S., Cassino, L.F., Alkmim, F.F., 2017. U–Pb
653 ages and Hf-isotope data of detrital zircons from the late Neoarchean-
654 Paleoproterozoic Minas Basin, SE Brazil. Precambrian Res. 291, 143–161.
655 https://doi.org/10.1016/j.precamres.2017.01.026
656 McKie, T., 1990. Tidal and storm influenced sedimentation from a Cambrian
657 transgressive passive margin sequence. J. Geol. Soc. London. 147, 785–794.
658 https://doi.org/10.1144/gsjgs.147.5.0785
659 Meinhold, G., Morton, A.C., Fanning, C.M., Whitham, A.G., 2011. U-Pb SHRIMP ages
660 of detrital granulite-facies rutiles: Further constraints on provenance of Jurassic
661 sandstones on the Norwegian margin. Geol. Mag. 148, 473–480.
662 https://doi.org/10.1017/S0016756810000877

663 Morton, A.C., Hallsworth, C., 1994. Identifying provenance-specific features of detrital
664 heavy mineral assemblages in sandstones. Sediment. Geol. 90, 241–256.
665 Mulder, J.A., Karlstrom, K.E., Halpin, J.A., Merdith, A.S., Spencer, C.J., Berry, R.F.,
666 McDonald, B., 2018. Rodinian devil in disguise: Correlation of 1.25-1.10 Ga strata
667 between Tasmania and Grand Canyon. Geology 46, 991–994.
668 https://doi.org/10.1130/G45225.1
669 Müller, S., Dziggel, A., Sindern, S., Kokfelt, T.F., Gerdes, A., Kolb, J., 2018. Age and
670 temperature-time evolution of retrogressed eclogite-facies rocks in the
671 Paleoproterozoic Nagssugtoqidian Orogen, South-East Greenland: Constrained
672 from U-Pb dating of zircon, monazite, titanite and rutile. Precambrian Res. 314,
673 468–486. https://doi.org/10.1016/j.precamres.2018.07.002
674 Nyberg, B., Gawthorpe, R.L., Helland-Hansen, W., 2018. The distribution of rivers to
675 terrestrial sinks: Implications for sediment routing systems. Geomorphology 316,
676 1–23. https://doi.org/10.1016/j.geomorph.2018.05.007
677 O'Sullivan, G.J., Chew, D.M., Samson, S.D., 2016. Detecting magma-poor orogens in
678 the detrital record. Geology 44, 871–874. https://doi.org/10.1130/G38245.1
679 Odlum, M.L., Stockli, D.F., Capaldi, T.N., Thomson, K.D., Clark, J., Puigdefàbregas, C.,
680 Fildani, A., 2019. Tectonic and sediment provenance evolution of the South
681 Eastern Pyrenean foreland basins during rift margin inversion and orogenic uplift.
682 Tectonophysics 765, 226–248. https://doi.org/10.1016/j.tecto.2019.05.008
683 Okay, N., Zack, T., Okay, A.I., Barth, M., 2011. Sinistral transport along the Trans-
684 European Suture Zone: Detrital zircon-rutile geochronology and sandstone
685 petrography from the Carboniferous flysch of the Pontides. Geol. Mag. 148, 380–
686 403. https://doi.org/10.1017/S0016756810000804
687 Pereira, I., Storey, C., Darling, J., Lana, C., Alkmim, A.R., 2019. Two billion years of
688 evolution enclosed in hydrothermal rutile: Recycling of the São Francisco Craton
689 Crust and constraints on gold remobilisation processes. Gondwana Res. 68, 69–
690 92. https://doi.org/S1342937X18303058

691 Robinson, D., 1987. Transition from diagenesis to metamorphism in extensional and
692 collision settings. Geology 15, 866–869. https://doi.org/10.1130/0091-7613
693 Rösel, D., Boger, S.D., Möller, A., Gaitzsch, B., Barth, M., Oalmann, J., Zack, T.,
694 2014a. Indo-Antarctic derived detritus on the northern margin of Gondwana:
695 Evidence for continental-scale sediment transport. Terra Nov. 26, 64–71.
696 https://doi.org/10.1111/ter.12070
697 Rösel, D., Zack, T., Boger, S.D., 2014b. LA-ICP-MS U–Pb dating of detrital rutile and
698 zircon from the Reynolds Range: A window into the Palaeoproterozoic
699 tectonosedimentary evolution of the North Australian Craton. Precambrian Res.
700 255, 381–400. https://doi.org/10.1016/j.precamres.2014.10.006
701 Santos, M., Lana, C., Scholz, R., BUICK, I., Schmitz, M.D., Kamo, S.L., Gerdes, A.,
702 Corfu, F., Tapster, S., Wiedenbeck, M., 2017. A New Appraisal of Sri Lankan BB
703 Zircon as Reference Material for LA- ICP-MS U-Pb Geochronology and Lu-Hf
704 Isotope Tracing. Geostand. Geoanalytical Res. 41, 335–358.
705 https://doi.org/10.1111/ijlh.12426
706 Saylor, J.E., Sundell, K.E., 2016. Quantifying comparison of large detrital
707 geochronology data sets 12, 203–220. https://doi.org/10.1130/GES01237.1
708 Schmitt, A.K., Zack, T., 2012. High-sensitivity U-Pb rutile dating by secondary ion mass
709 spectrometry (SIMS) with an O^{2+} primary beam. Chem. Geol. 332–333, 65–73.
710 https://doi.org/10.1016/j.chemgeo.2012.09.023
711 Stewart, A., 2002. The late Proterozoic Torridonian rocks of Scotland; their
712 sedimentology, geochemistry and origin, Journal of the geological Society
713 Memoirs no 24.
714 van Gool, J.A.M., Rivers, T., Calon, T., 2008. Grenville Front zone, Gagnon terrane,
715 southwestern Labrador: Configuration of a midcrustal foreland fold-thrust belt.
716 Tectonics 27, 1–35. https://doi.org/10.1029/2006TC002095
717 Wiedenbeck, M., Allé, P., Corfu, F., Griffin, W.L., Meier, M., Von Quadt, A., Roddick,
718 J.C., Spiegel, W., 1995. Three natural zircon standards for U-Th-Pb, Lu-Hf,

element and REE analyses. Geostand. Newsl. 19, 1–23.

Zack, T., Stockli, D.F., Luvizotto, G.L., Barth, M.G., Belousova, E., Wolfe, M.R., Hinton, R.W., 2011. In situ U-Pb rutile dating by LA-ICP-MS: ^{208}Pb correction and prospects for geological applications. Contrib. to Mineral. Petrol. 162, 515–530. https://doi.org/10.1007/s00410-011-0609-4

Graphical Abstract

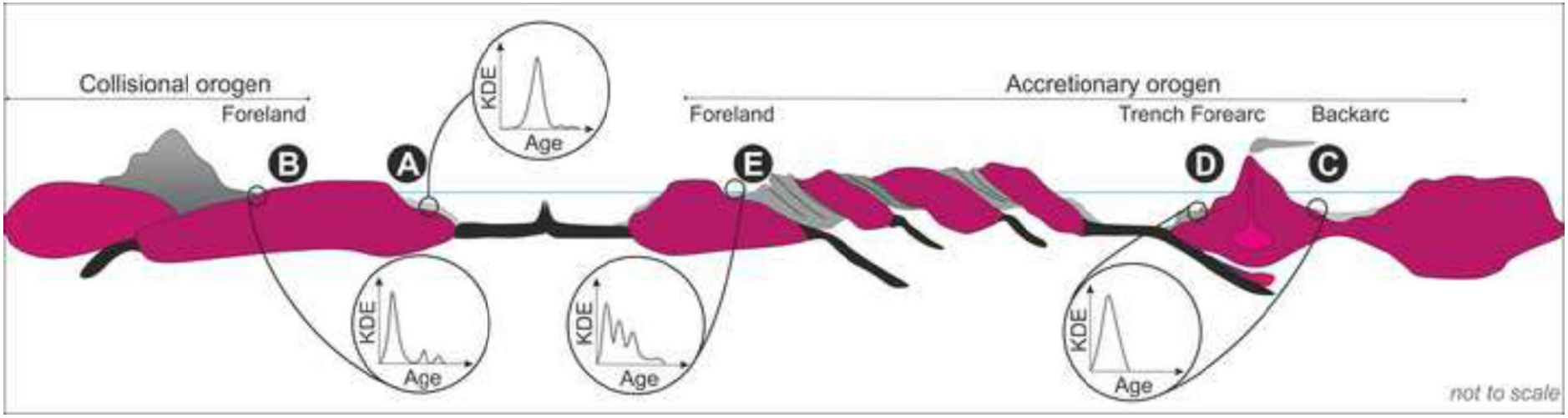

Captions Fig and table
Click here to download Figure: Captions.docx

Figure 1. Detrital rutile and zircon KDE examples of a) extensional settings (data from Fielding et al. 2018 from an extensional basin) showing a gaussian unimodal distribution of rutile against a multivariate distribution of detrital zircon, indicating inheritance; b) collisional orogen (data from Bracciali et al., 2016, 2015 from the Himalayas foreland) showing differences in the rutile and zircon KDE. Data include only the 95-105% concordant data, and ages are either $^{206}Pb/^{238}U$ for ages <1000 Ma and $^{207}Pb/^{206}Pb$ for ages >1000 Ma.

Figure 2. Schematic model of different tectonic environments and corresponding detrital rutile KDE curves associated with those basins, namely A-passive margin, B-collisional foreland, C-back-arc, D- trench and fore-arc, and E- accretionary foreland.

Figure 3. Cumulative proportion distributions against growth – deposition ages diagram, modified from Cawood et al. (2012). Coloured fields correspond to different depositional tectonic settings: A. convergent basins, B. collisional basins, C. extensional basins. White dashed lines highlight overlapping fields from different tectonic environments. Two different datasets are projected, with data from Rosël et al. (2014b) and Lippert (2014), corresponding to a backarc and an accretionary foreland basin, respectively. Coloured curves correspond to detrital rutile distribution, and grey curves to detrital zircon. Black arrows indicate significant differences in the cumulative proportions between detrital rutile and zircon from the same dataset for the same age interval. These curves show how detrital zircon cumulative probability distribution curves plot in ambiguous fields, such as the foreland data, projected in the extensional field, whilst detrital rutile from the same sequence are projected in the collisional field.

Figure 4. Depositional tectonic setting diagram based on detrital rutile for **A.** extensional settings, with data from 1. Rosel et al. (2014a), 2. Meinhold et al. (2011), 3. O'Sullivan et al. (2016), 4. Fielding et al. (2018). 'S' curve age distributions correspond to extensional settings; **B**. Transition between rift and passive margin detrital rutile age distribution curves in 'suture rift' basins. Arrow points to the period where each curve shows an inflection. Data from Avigad et al. (2017).

Figure 5. Depositional tectonic setting diagram based on detrital rutile for convergent-collisional settings, with data from 1.Rösel et al. (2014b), 2.Okay et al. (2011), 3.Bracciali et al. (2016), 4. and 5.Lippert (2014) Utah and Wyoming sequences, respectively. This allows distinction of convergent and continental foreland basins from foreland basins developed on the accreting side of the orogen. "r" shape age distributions curve corresponding to convergent settings. White dashed line in the diagram marks the age of the exposed basement due to the out of sequence thrusting in the Sevier Foreland (USA).

Figure 6. Rutile and zircon U-Pb age data diagrams for the Torridon Group. KDE and histogram frequency distribution, and cumulative probability of detrital rutile (red; light grey) and zircon (blue, dark grey) for the Diabaig Formation (**A** and **C**, respectively); and for the Applecross Formation (**B** and **D**, respectively). Zircon data for the Diabaig Formation come from this study and Kinnaird et al. (2007), and for the Applecross Formation come from Lancaster et al. (2011) and Krabbendam et al. (2017). Rutile data for the

Diabaig Formation come from this study and for the Applecross Formation from this study combined with data from Krabbendam et al. (2017).

Figure 7. Rutile and zircon U-Pb age data diagrams for the Ardvreck Grp. KDE and histogram frequency distribution, and cumulative probability of detrital rutile (red/light grey) and zircon (blue/dark grey) for Basal Quartzite Mbr. (**A** and **C**, respectively); and for Pipe Rock Mbr. (**B** and **D**, respectively). Zircon data come from Cawood et al. (2007) and Lancaster et al. (2011).

Figure 8. U-Pb rutile data retrieved from the metaconglomerate unit of the Sabará Formation; A. Wetherill Concordia showing a Palaeoproterozoic upper intercept and a Pb-loss Palaeozoic lower intercept. These data suggest the existence of a major population at around 2.15 Ga affected by a tectonothermal event at 490 Ma; B. Rutile and zircon U-Pb age data diagrams for the Sabará metaconglomerate. KDE and histogram frequency distribution, and cumulative probability of detrital rutile (red/light grey) and zircon (blue/dark grey); C. Cumulative probability curves for detrital rutile and zircon using $^{207}Pb/^{206}Pb$ ages. Both represent a steep curve with a small gap between deposition age and the main population ages.

Figure 9. Depositional tectonic setting diagram based on detrital rutile for **A.** extensional settings, with data from 1. Rosel et al. (2014a), 2. Meinhold et al. (2011), 3. O'Sullivan et al. (2016), 4. Fielding et al. (2018), and from this study, 5. Ardvreck Grp (NW Scotland); **B.** convergent-collisional settings, with data from 1.Rösel et al. (2014b), 2.Okay et al. (2011), 3.Bracciali et al. (2016), 4. and 5.Lippert (2014), and from this study, 6.Sabará Grp. (Brazil) and 7. Torridon Grp (NW Scotland).

Table 1. Summary of the statistical test results obtained using DZstats (Saylor and Sundell, 2016). Rut for rutile, zir for zircon; APC – Applecross, DIA – Diabaig, PR – Pipe Rock, BQ – Basal Quartzite formations.

Figure 1
Click here to download high resolution image

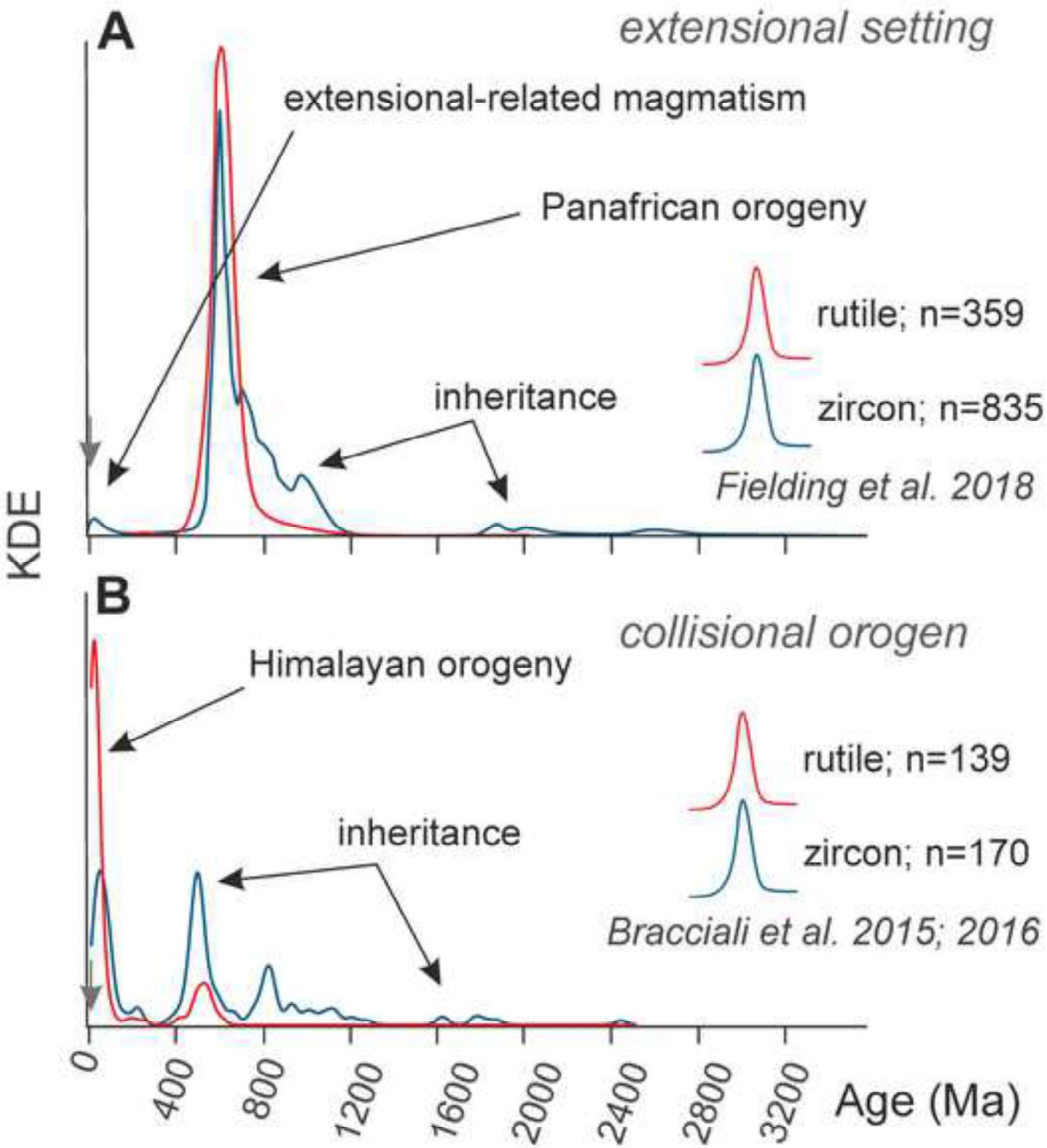

Figure 2
Click here to download high resolution image

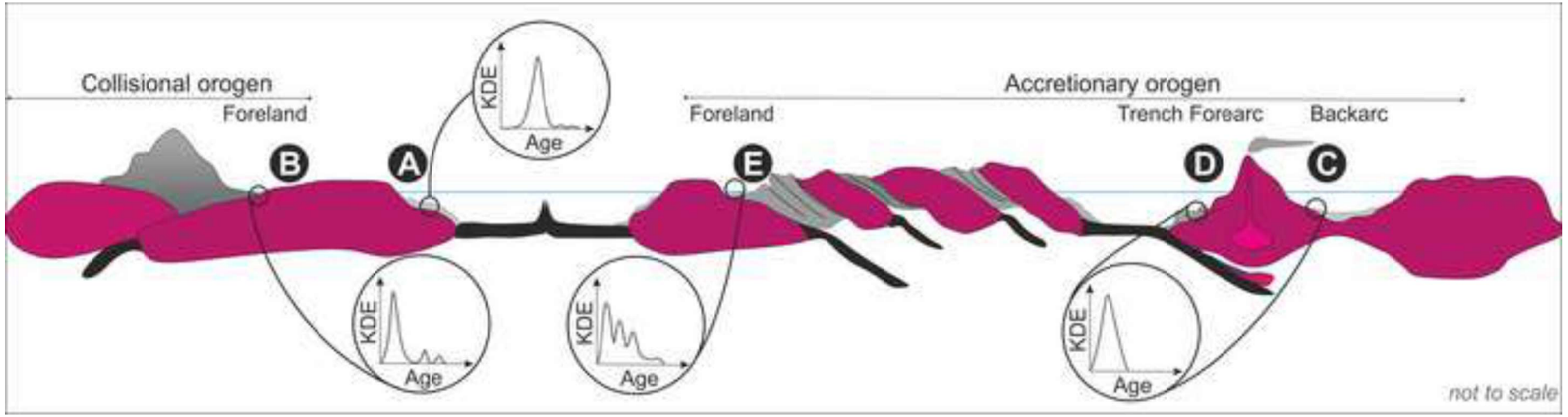

Figure 3
Click here to download high resolution image

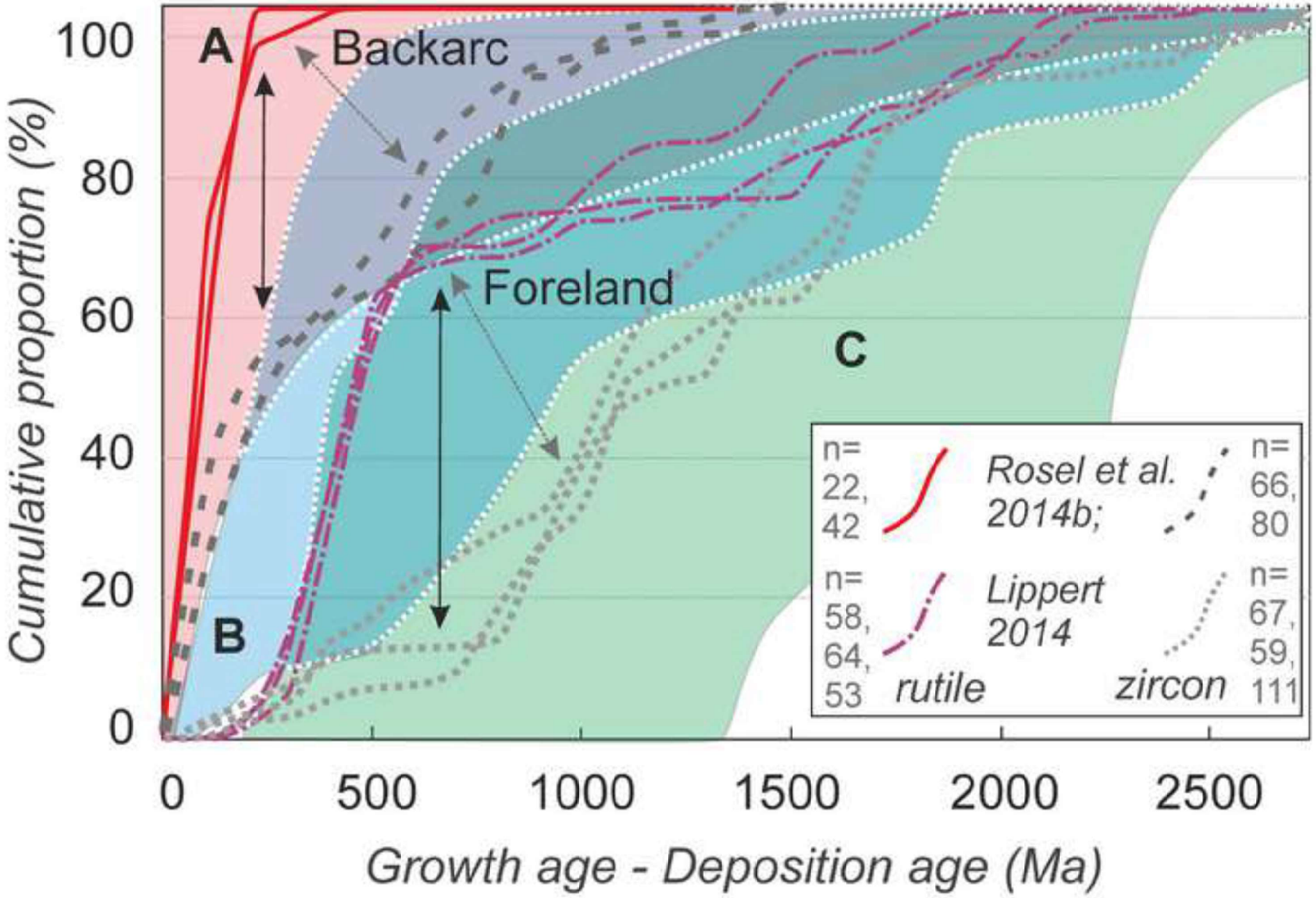

Figure 4

Click here to download high resolution image

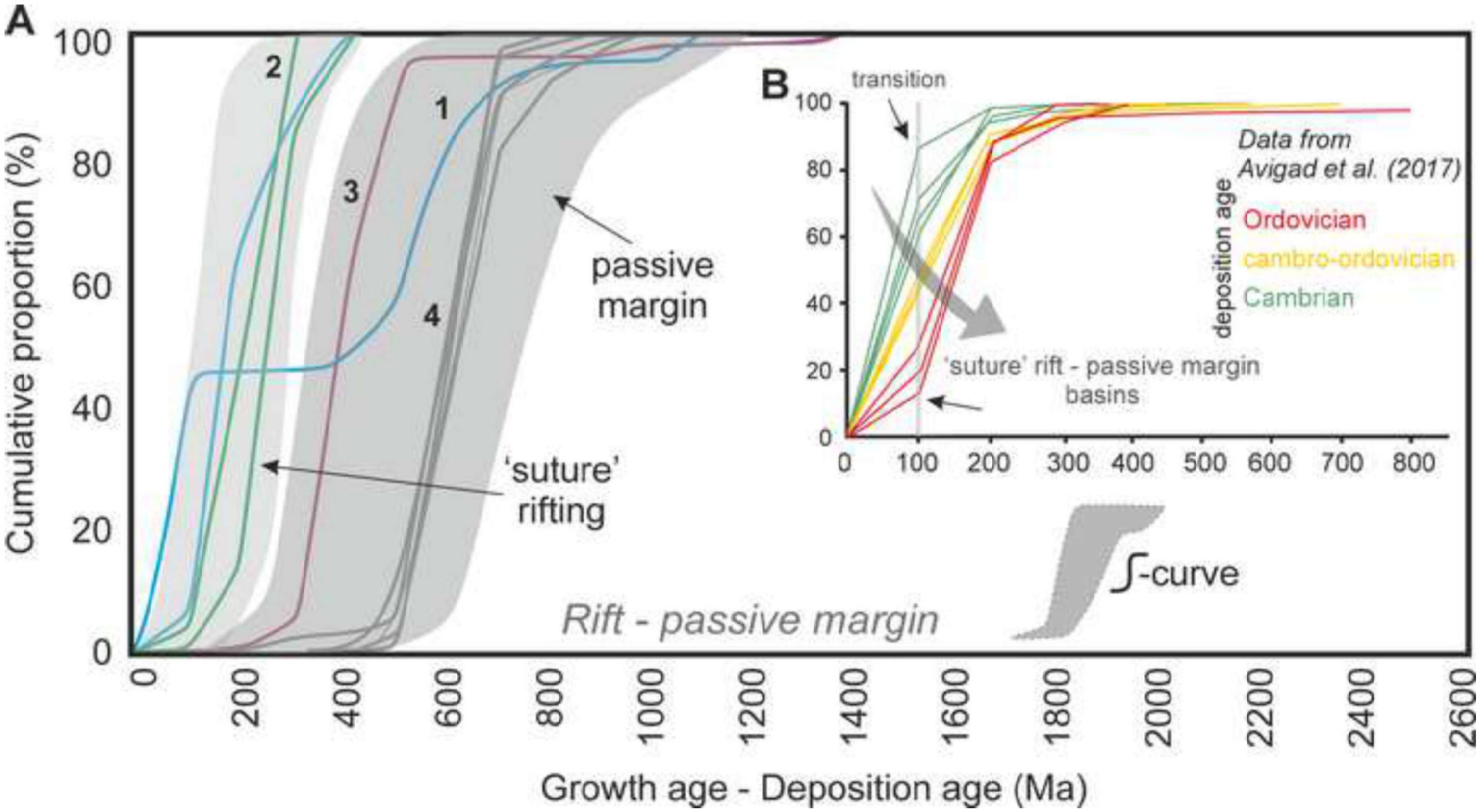

Figure 5

Click here to download high resolution image

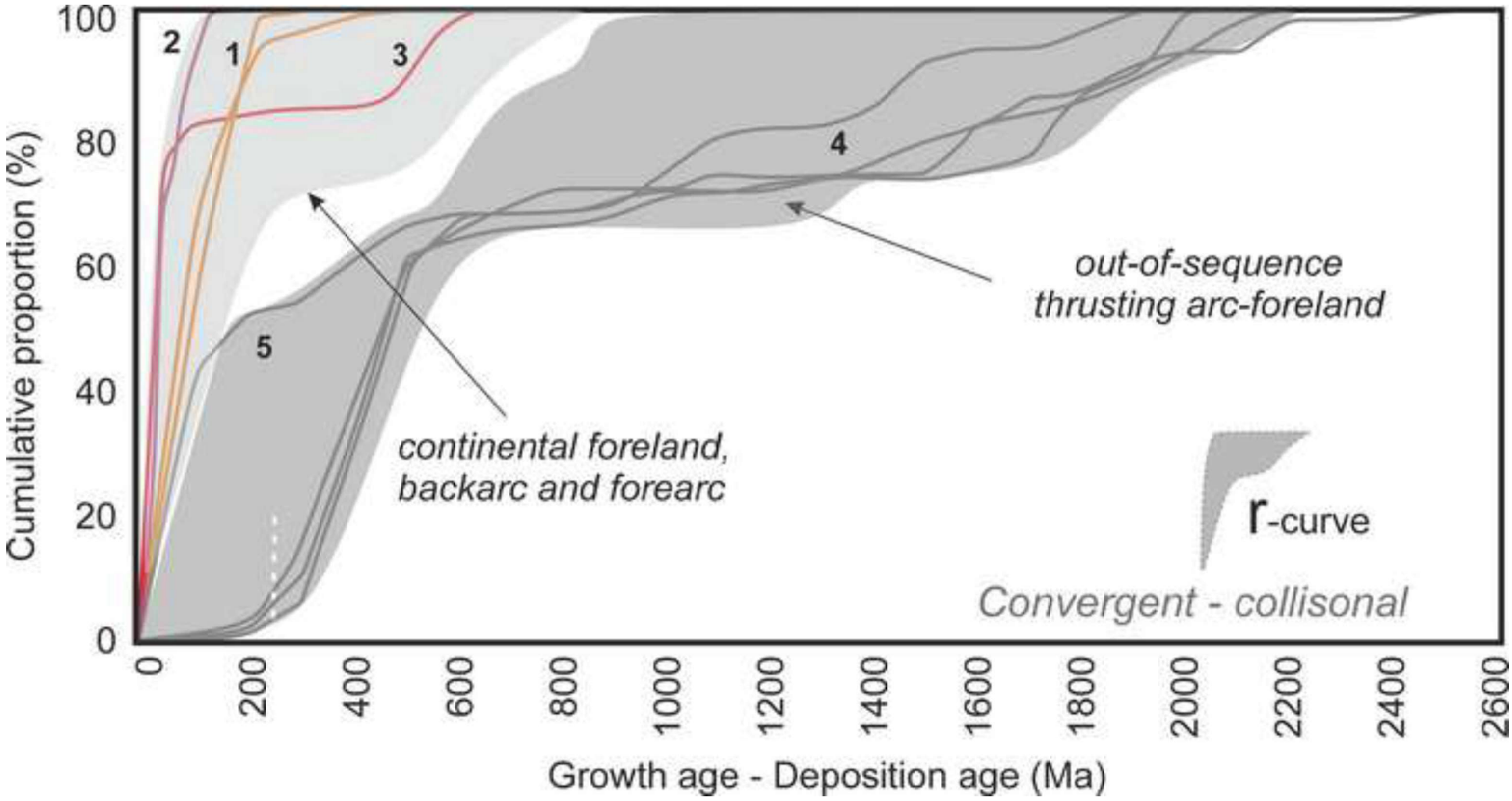

Figure 6

Click here to download high resolution image

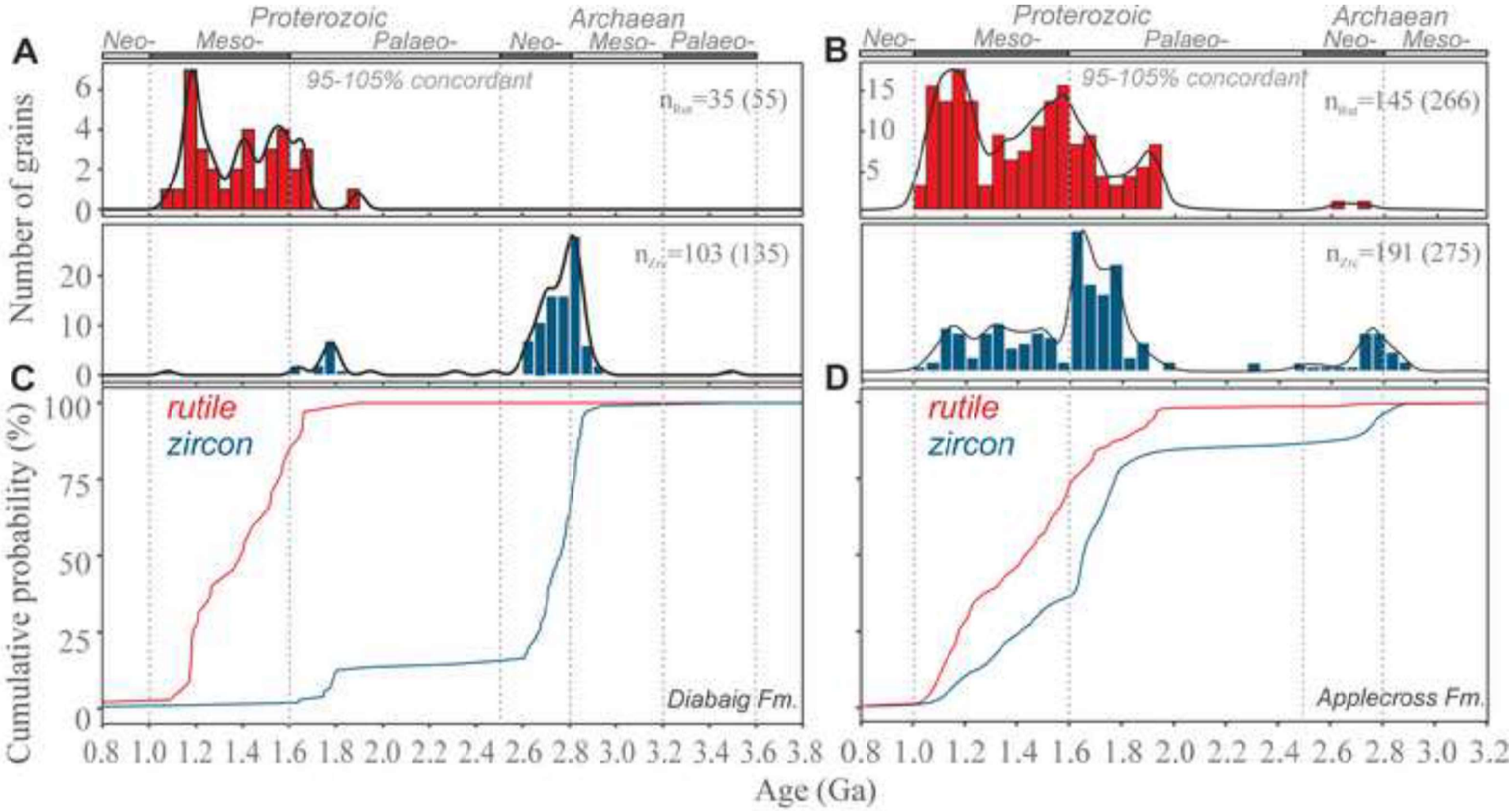

Figure 7

Click here to download high resolution image

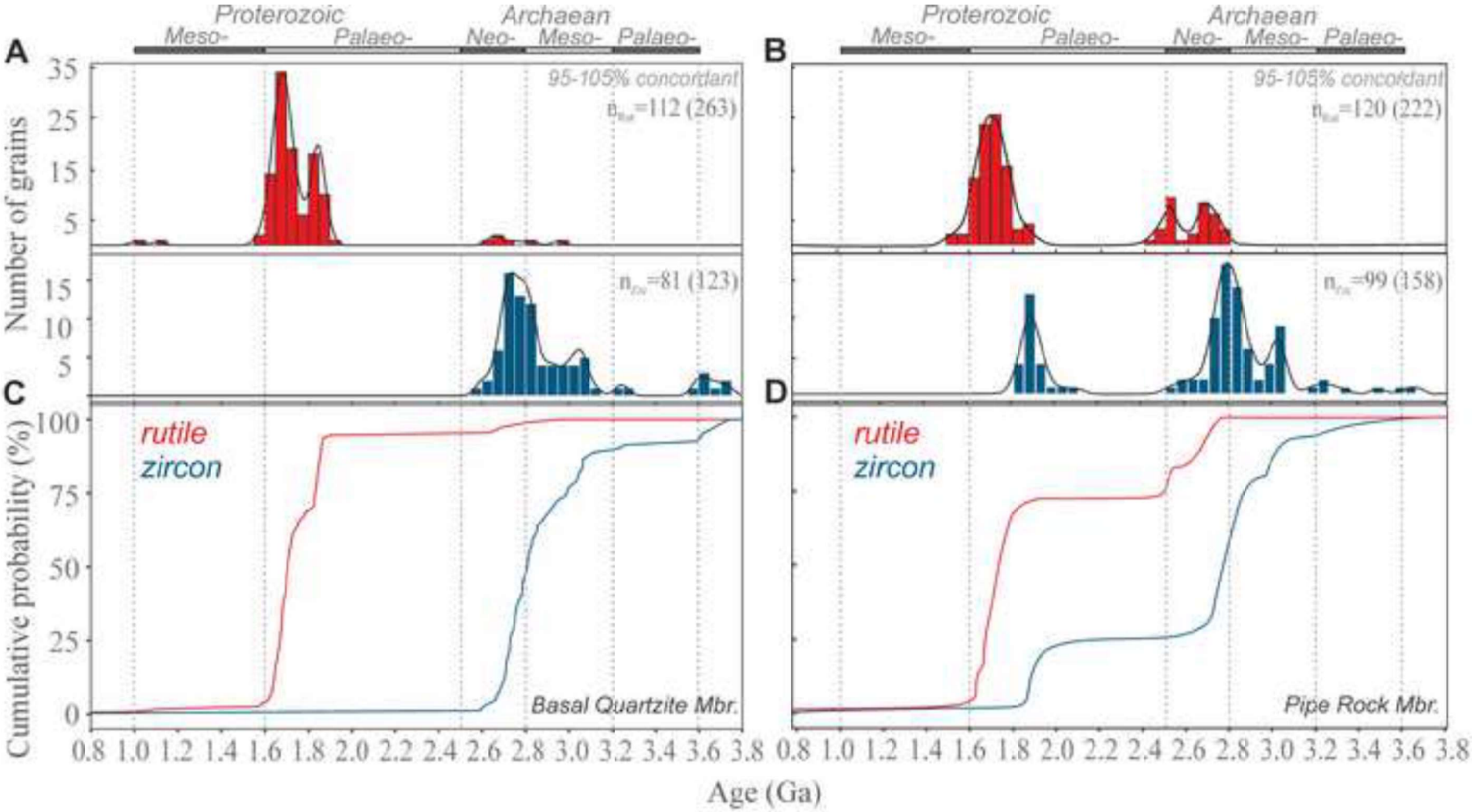

Figure 8

Click here to download high resolution image

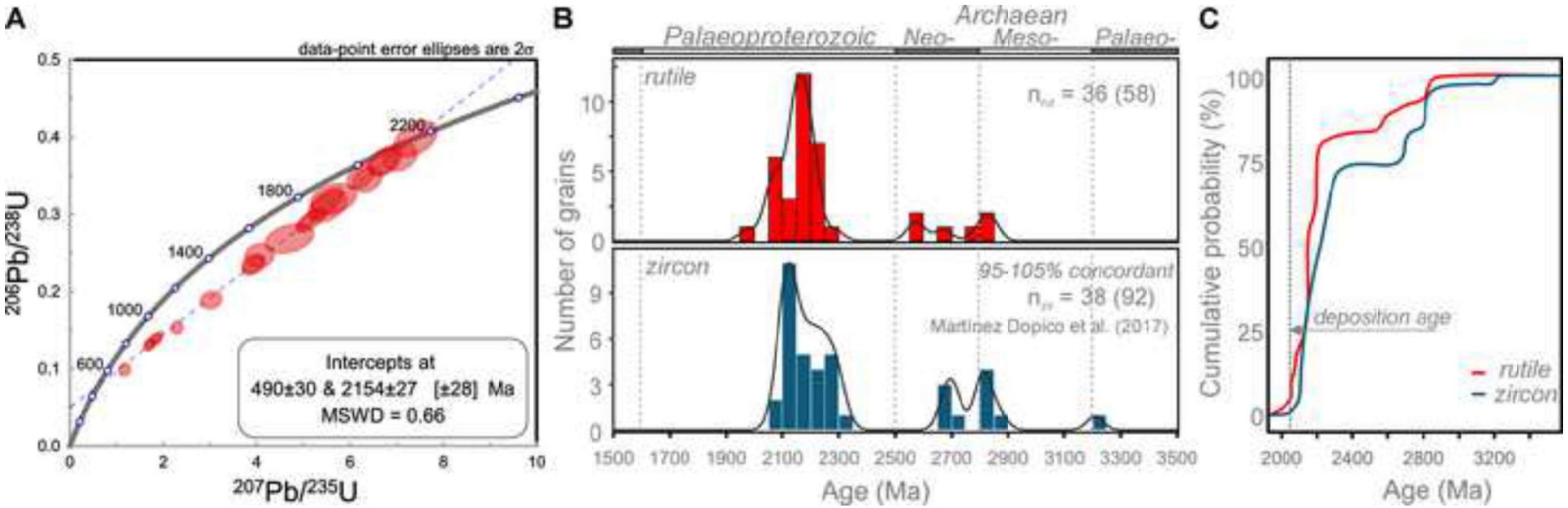

Figure 9
Click here to download high resolution image

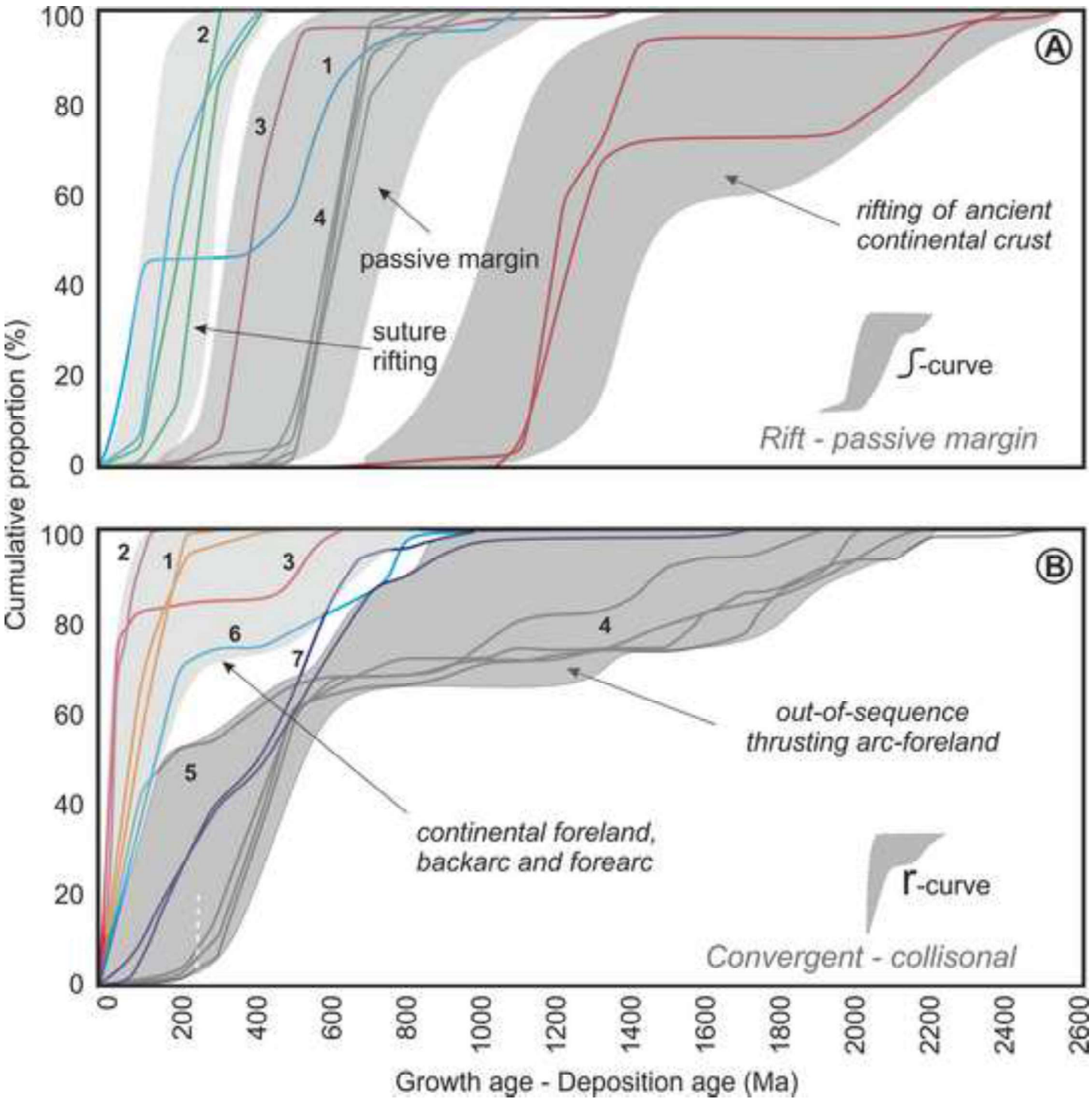

Table 1

Click here to download Table: Table 1.docx

Populations / test	Cross-correlation KDE	Likeness KDE	Cross-correlation PDP	Similarity PDP
Applecross rut-zir	0.406	0.607	0.295	0.834
Diabaig rut-zir	0.014	0.087	0.009	0.099
Pipe Rock rut-zir	0.006	0.245	0.002	0.393
Basal Q. rut-zir	0.004	0.053	0.004	0.185
APC-DIA rut	**0.9**	**0.851**	**0.66**	**0.903**
PR-BQ rut	**0.699**	**0.635**	**0.736**	**0.871**
APC-DIA zir	0.047	0.276	0.038	0.538
PR-BQ zir	**0.722**	**0.728**	0.586	**0.801**